*metals*

MDPI

*Review*

# Grain Refinement of Aluminum and Aluminum Alloys by Sc and Zr

**Zhiguo Lei, Shengping Wen *, Hui Huang, Wu Wei and Zuoren Nie**

Faculty of Materials and Manufacturing, Beijing University of Technology, Beijing 100124, China
* Correspondence: wensp@bjut.edu.cn

**Abstract:** Rare earth elements and transition elements are widely used in aluminum alloys, magnesium alloys and copper alloys due to their unique microalloying effects. With regard to in-depth research on the grain refinement characteristics of rare earth elements and transition elements, the combination of grain refinement and microalloying in the master alloys has a great impact on the theories and technical research of refinement, and the broadening of the application field of master alloys. This paper first summarizes the grain refinement mechanisms and analyzes the effects of rare earth elements and transition elements on the grain refinement of aluminum and aluminum alloys, and summarizes the elements suitable for the preparation of Al-M master alloys and their refinement mechanism.

**Keywords:** aluminum alloys; Sc; Zr; heterogeneous nucleation; edge to edge matching model; grain refinement; microalloying

check for updates

**Citation:** Lei, Z.; Wen, S.; Huang, H.; Wei, W.; Nie, Z. Grain Refinement of Aluminum and Aluminum Alloys by Sc and Zr. *Metals* **2023**, *13*, 751. https://doi.org/10.3390/met13040751

Academic Editor: Sergey V. Zherebtsov

Received: 27 February 2023
Revised: 7 April 2023
Accepted: 11 April 2023
Published: 12 April 2023

**Copyright:** © 2023 by the authors. Licensee MDPI, Basel, Switzerland. This article is an open access article distributed under the terms and conditions of the Creative Commons Attribution (CC BY) license (https://creativecommons.org/licenses/by/4.0/).

## 1. Introduction

Aluminum and its alloys are highly attractive engineering materials for structural applications in many industries due to their low density, high specific strength and good corrosion resistance [1–3]. With the development of material technology, higher requirements have been put forward for the comprehensive properties of aluminum alloys, namely to obtain aluminum alloys with higher strength and better thermal stability [4]. The properties of aluminum alloys are controlled by a number of microstructural characteristics, such as grain size. Grain refinement, by promoting nucleation [5,6] and growth restriction [7], obtains a fine equiaxed crystal structure of α-Al, eliminates columnar structure, ensures uniform mechanical properties, improves formability and machinability, reduces casting defects and tearing tendency, and enhances subsequent machining response [8–10].

The grain refinement of commercial aluminum and aluminum alloys is mainly regulated by grain refiners [11]. Grain refiners are a type of master alloys. When the grain refining master alloys are added to melt, a large number of heterogeneous nucleating cores are released after melting. Those cores can affect the nucleating process of melt crystallization by acting as external cores during melt solidification, and play the role of refining grains. The most popular grain refiners are Al-Ti-B master alloys [12,13]. However, Al-Ti-B has no other effect after grain refinement, such as microalloying. Based on the Edge To Edge matching model [14,15] (E2E model), the coherent relationship between the two phases was determined by calculating the mismatch degree of the close-packed crystal plane and the close-packed crystal direction. A class of heterogeneous phase $Al_2RE$ (Rare Earth element) with a refining effect was screened for magnesium alloys. This phase can also improve the thermal stability of the microstructure [16–19]. In 2009, Qin et al. [16] added 0.6%~1.0 wt.%Al to Mg-10Y alloy, and the $Al_2Y$ formed by Y and Al in the melt reduced the grain size of the alloy from 180 μm to 36 μm. The size reduction rate was up to 80%, and the refinement effect was almost similar to that of adding Zr. $Al_2Y$ is a compound with high thermal stability, and the microstructure thermal stability of $Al_2Y$ is stronger

than that of Zr-added magnesium alloy due to its uniform distribution within the grain and at the grain boundary, which can effectively hinder grain boundary migration.

Considering the heterogeneous phase $Al_2RE$, which has the function of refining magnesium alloy grains and microalloying, we draw on this idea and plan to design an Al-M (Metal) master alloy for the field of aluminum alloys, which both refines grain and improves thermal stability of the microstructure. Transition element Hf is a good example. When Hf is added to pure aluminum, the primary phase $Al_3Hf$ with $L1_2$ structure can be formed, and the primary phase can also pin the grain boundary after heterogeneous nucleation [20]. Sc, Zr and Er are often used as microalloying elements combined with Al to form the $Al_3M$ phase to improve the mechanical properties and heat resistance of aluminum alloys [21–26]. Literature review shows that rare earth elements and transition elements can form the $Al_3M$ phase with Al after solidification to refine the α-Al grains of aluminum castings, improve the microstructure and obtain equiaxed grains [20,27–33]. Therefore, it is of great practical significance to study the grain refinement law, refinement mechanism and factors affecting the refinement effect of rare earth elements and transition elements to supplement the grain refinement theory and expand the application field of rare earth elements and transition elements. The application range of Al-M master alloys can be further expanded by combining the refined grains of elements with microalloying.

In this paper, the current mainstream grain refinement theory is summarized. Based on the generalized grain refinement theory [34–41], the refining mechanism and refining effect of rare earth elements and transition elements on the grains of aluminum and aluminum alloy are analyzed. The elements suitable for the preparation of an Al-M master alloy and their refining mechanism and influencing factors of refinement effect are summarized. Finally, the problems existing in the research process of Al-M intermediate alloys are presented.

## 2. The Mechanism of Grain Refinement

Based on a large number of studies [12,28,34–36,38,42–45], the theory of grain refinement on grain refinement of aluminum alloy refiners can be divided into constitutional supercooling of solute atoms and heterogeneous nucleation. Grain refiners refine grains mainly by promoting grain nucleation or inhibiting grain growth. Constitutional supercooling provides subcooling and inhibits grain growth. Heterogeneous phases provide a large number of nucleation sites, improve the nucleation rate and eventually lead to grain refinement. Both mechanisms are explained in detail below.

### *2.1. Constitutional Supercooling*

During the solidification process of alloys, the segregation of supersaturated solute atoms from the grains leads to a decrease in constitutional supercooling at the front of the solid–liquid interface and the inhibition of grain growth. This phenomenon is called compositional undercooling [36]. When the supercooling degree ($\Delta T_C$) provided by solute segregation is greater than the critical subcooling degree ($\Delta T_n$) required for nucleation, migration at the solid–liquid interface is hindered, and continued growth of original grains is also inhibited, which induces grain refinement. The ability of solute elements to inhibit grain growth is usually quantified by the Growth Restriction Factor (GRF for short, also known as $Q$). Easton and Stjohn [36] used GRF to quantitatively describe the inhibition effect of different solute elements on grain growth in cast alloys. The expression for calculating the growth restriction factor is as follows:

$$Q = mC(k-1) \tag{1}$$

where $m$ is the liquidus slope of the aluminum-rich end of the binary alloy, $C$ is the solubility of the solute and $k$ is the solute partition coefficient (e.g., $k = \frac{C_S}{C_L}$, $S$ represents the α-Al phase and $L$ represents the liquid phase, $C_S$ is the maximum solid solubility of the aluminum-rich end of the binary alloy and $C_L$ is represents peritectic point or eutectic point).

Generally speaking, for the liquidus slope of the Al-rich end of eutectic reactive binary alloys, $m$ is negative, and the $k$ value is less than 1. For peritectic reaction type binary alloy, $m$ is positive, and the $k$ value is greater than 1. Plug $m$, $k$ and $C$ into Formula 1, so that $Q$ is always positive. For solute elements that do not interact with each other, their influence on the solidification process can be measured by the sum of the growth limiting factors of various solutes ($\sum Q$). Table 1 shows the theoretical growth-limiting factors of different solute elements during alloy solidification. According to the Table 1, the Ti element has the highest value of $Q/C$, and has the best grain growth inhibition effect and can produce the best grain refinement effect under the same mass percentage content. Johnsson [46] studied the subcooling of Ti components and found that the larger $Q$, the better the grain refinement effect. When $Q$ is 7, the grain size of pure aluminum is 250 μm. When $Q$ increases to 23, the grain size decreases to 120 μm.

**Table 1.** Parameters underlying the calculation of $Q$ for different solutes in aluminum [47].

| Element | System | $m$ (K/wt.%) | $K$ | $C$ (wt.%) | $Q/C$ (K/wt.%) |
|---|---|---|---|---|---|
| Cu | eutectic | −3.4 | 0.17 | 33.2 | 2.8 |
| Ni | eutectic | −3.3 | 0.007 | 6 | 3.3 |
| Mg | eutectic | −6.2 | 0.51 | 3.4 | 3.0 |
| Mn | eutectic | −1.6 | 0.94 | 1.9 | 0.1 |
| Si | eutectic | −6.6 | 0.11 | 12.6 | 5.9 |
| Fe | eutectic | −3.0 | 0.02 | 1.8 | 2.9 |
| Er | eutectic | −0.91 | 0.03 | 6 | 0.88 |
| Sc | eutectic | −9.4 | 0.59 | 0.58 | 3.90 |
| Ti | peritectic | 7.8 | 33.3 | 0.15 | 220 |
| Cr | peritectic | 3.5 | 2.0 | 0.4 | 3.5 |
| Ta | peritectic | 70.0 | 7.8 | 0.10 | 105 |
| V | peritectic | 10.0 | 4.0 | 0.1 | 30.0 |
| Hf | peritectic | 8.0 | 2.4 | 0.5 | 11.2 |
| Mo | peritectic | 5.0 | 2.5 | 0.1 | 7.5 |
| Nb | peritectic | 13.3 | 1.5 | 0.15 | 6.6 |
| Zr | peritectic | 4.5 | 2.5 | 0.11 | 6.8 |

In addition to the data found in reference [47], this document strengthens the table with more information.

### *2.2. Heterogeneous Nucleation*

In addition to the constitutional supercooling mechanism of solute atoms, elements also exist in the form of phases, which should also be considered as heterogeneous nucleation. The mechanism of heterogeneous nucleation is based on the crystallographic relationship between the heterogeneous phase and matrix. There are three prevailing views: the lattice matching principle [40], two-dimensional matching model [39] and Edge To Edge matching model [14,15,43,48].

#### 2.2.1. Lattice Matching Principle

Traditional heterogeneous nucleation theory holds that the distinguishing condition for heterogeneous particles to exert nucleation effect is that there is a small interfacial energy between the particle and matrix phase. The mismatch degree between the heterogeneous phase and matrix, the electrostatic potential, and the morphology, size and size distribution of the heterogeneous phase are all factors affecting the interfacial energy, among which the mismatch degree is the dominant factor affecting the nucleation efficiency of the heterogeneous phase. The mismatch degree between the heterogeneous phase and the matrix is widely used to measure its refining ability or to find new nucleating particles. According to the solidification theory, the smaller the lattice mismatch between particles and matrix, the lower the interfacial energy of two phases and the stronger the heterogeneous nucleation effect of particles. Initially, based on lattice constants, Turnbull and Vonnegut [40] theoretically studied the lattice mismatch degree between matrix and nucleated particle, and proposed the formula of mismatch degree ($\delta$):

$$\delta = \frac{\Delta a_0}{a_0} \tag{2}$$

where $\Delta a_0$ is the difference between the lattice constant of the matrix and the particle on the low index crystal plane and $a_0$ is the lattice constant of the matrix.

The model points out that when $\delta \leq 15\%$, the nucleation particle can produce a refining effect, otherwise there is no refining ability.

Based on the lattice matching theory, Bramfitt [39] established two-dimensional lattice matching model to make the low index crystal planes of nucleating particles and matrix phases coincide, which can be applied to the calculation of the mismatch between two phases of crystal planes with different atomic arrangement. The formula for calculating the two-dimensional mismatch ($\delta \frac{(hkl)_s}{(hkl)_n}$) is as follows:

$$\delta \frac{(hkl)_s}{(hkl)_n} = \frac{1}{3}\sum_{i=1}^{3} \frac{\left| d[uvw]_s^i \cos\theta - d[uvw]_n^i \right|}{d[uvw]_n^i} \times 100\% \quad (3)$$

where $s$ is the matrix and $n$ is the nucleating particle. $(hkl)$ is low index crystal facet; $[uvw]$ is the low index orientation on the low index crystal plane; $d[uvw]_s$ and $d[uvw]_n$ are the atomic spacing along the corresponding crystal plane and the crystal direction, respectively; $\theta$ is the angle between the crystal direction of $[uvw]_s$ and $[uvw]_n$. The theory states that heterogeneous nucleation is effective when $\delta < 6\%$. If $\delta$ = 6%–12%, it has medium efficacy; if it is more than 12%, granules cannot be used as heterogeneous nucleation cores. The face mismatch degree between $Al_4C_3$ and Mg matrix is 4.05% [46]. Subsequent experiments show that $Al_4C_3$ particles can significantly refine the as-cast grains of magnesium alloy, which fully verifies the effectiveness of the surface matching model.

Based on previous research results, Zhang et al. [14,15] proposed the E2E model to consider the mismatch degree from the perspective of atomic row (crystal direction) at the phase interface. The key assumption of the E2E model is that the nucleation substrate always occurs at the orientation with the least mismatch when the atomic row at the two-phase interface is parallel and the mismatch degree is minimum. For the requirement of atomic columns, the atomic columns satisfying the hypothesis should first be densely or nearly densely packed; secondly, the atomic columns can be arranged in straight lines (abbreviated as S) or zig-zag lines (abbreviated as Z), as shown in Figure 1. Finally, the lines of straight atoms correspond to the lines of straight atoms, and the lines of sawtooth atoms correspond to the lines of sawtooth atoms.

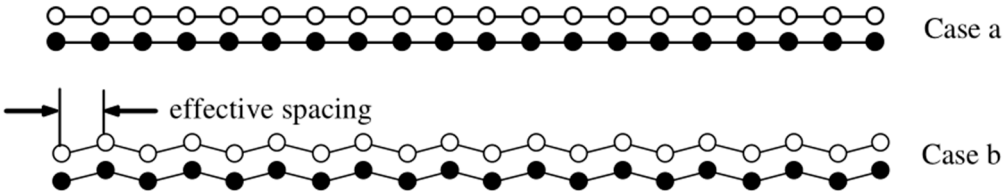



**Figure 1.** Schematic illustration of two different types of atom row matching at the interface. Reprinted with permission from [15], 2005, Elsevier.

The E2E model quantifies the heterogeneous nucleation ability of particles using two parameters, namely interatomic spacing mismatch (it also known as $f_r$) and interplanar spacing mismatch (it also known as $f_d$), which correspond to the orientation and plane of crystal structure, respectively. When the $f_d$ and $f_r$ of nucleation substrate and primary crystal nucleus in a certain orientation are less than 6% and 10%, respectively, the nucleation substrate is an effective heterogeneous core. The atomic spacing mismatch ($f_r$) and crystal plane spacing mismatch ($f_d$) between phases can be calculated using the formula. The specific calculation formula is as follows:

$$f_d = \left| \frac{d_m - d_p}{d_m} \right| \times 100\% \quad (4)$$

$$f_r = \left| \frac{r_m - r_p}{r_m} \right| \times 100\% \quad (5)$$

where $d_m$ is the crystal plane spacing of matrix phase densely packed or nearly densely packed, $d_p$ is the crystal plane spacing of heterogeneous phase densely packed or nearly densely packed, $r_m$ is the atomic spacing of the matrix phase packed or nearly packed and $r_p$ is the atomic spacing of the heterogeneous phase packed or nearly packed.

The reliability of E2E model to predict refinement potential has been verified [42,43,48]. Wang [28] calculated the possible orientation relationship between $Al_3Zr$ phase and α-Al using the E2E model, and found that there are 6 groups of orientation relationships between $Al_3Zr$ and α-Al, and the mismatch degree is less than 6%. The orientation relationships of $[1\bar{1}0]_{Al_3Zr}(114)_{Al_3Zr}//[101]_{Al}(11\bar{1})_{Al}$ and $[40\bar{1}]_{Al_3Zr}(114)_{Al_3Zr}//[1\bar{1}0]_{Al}(11\bar{1})_{Al}$ were verified using EBSD (Electron Backscatter Diffraction), indicating that $Al_3Zr$ is indeed a heterogeneous core promoting α-Al nucleation. Li et al. [43] used the E2E model to predict whether $LaB_6$ had the potential to be a heterogeneous nucleating substrate of nascent $Al_{13}Mn_4Si_8$, and reached similar conclusions.

#### 2.2.2. Free Growth Model

In addition to the mismatching degree of interfacial atomic row, heterogeneous particle size is also a key factor affecting the heterogeneous nucleation efficiency [37,49–51]. When particle size met the conditions, the undercooling degree could be reduced to provide driving force and promote heterogeneous nucleation.

$$d_n = \frac{4\sigma_{SL}}{\Delta S_v \Delta T_n} \quad (6)$$

where $d_n$ is particle diameter (assumed to be spherical); $\sigma_{SL}$ is solid–liquid interface energy, about 158 mJ·m$^{-2}$ [37]; $\Delta S_v$ is the melting entropy per unit volume ($\Delta S_v$ is the ratio of melting potential heat $L_v$ to melting point $T_m$), which is determined to be $1.112 \times 10^6$ J·K$^{-1}$·m$^{-3}$ [37] in the experiment; $\Delta T_n$ is the critical degree of nucleation subcooling. Greer et al. [37,52,53] used the free growth model to study the grain refining effect of Al-Ti-B intermediate alloy, and found for the first time the quantitative relationship between the size of $TiB_2$ particles and the final grain refining effect. Greer et al. believed that larger $TiB_2$ particles preferentially act as nucleation cores to promote α-Al nucleation in the crystallization process. With the decrease in the melt temperature, the degree of supercooling increases, and smaller $TiB_2$ particles begin to produce a heterogeneous nucleation effect. At the same time, the latent heat release of crystalline grains leads to a slow decrease in temperature. No new grains are formed, and the smaller $TiB_2$ particles cannot serve as an effective nucleating core. Similarly, Yu et al. [54] analyzed the size change of $Al_3Ti$ in ECAP (Equal Channel Angular Pressing). After 10 ECAP deformations, when the size of $Al_3Ti$ particles remained in the optimal size range of 18–22 μm, the grain refinement performance of pure Al in the study object was the best and stable.

## 3. Al-M Master Alloy

Rare earth elements represented by Sc and Er, and transition elements represented by Zr are added to aluminum alloy in the form of master alloys. Nano-scale $Al_3M$ phase precipitated from the supersaturated solid solution of α-Al plays an important role in improving the recrystallization temperature of the aluminum alloy, and its mechanical properties and heat resistance [55]. A large number of studies [28,56–60] have shown that the three elements Sc, Zr and Er can also improve the casting microstructure and refine the grain. Considering that refiners in the field of magnesium alloy can play the role of refining grain and microalloying, we reference this idea. The existing research results of grain refinement of rare earth elements and transition elements are analyzed, and the elements suitable for developing Al-M master alloys with microalloying and grain refinement are summarized. Finally, the existing problems of Al-M master alloys are described.

### *3.1. Al-Sc*

The Sc element is often used as a microalloying element to improve the microstructure and properties of aluminum alloys. When Sc is added to aluminum alloy, after solid solution and aging treatment, the supersaturated solid solution α-Al is decomposed into $Al_3Sc$ precipitated phase with $L1_2$ structure. This is evenly and finely dispersed in the aluminum matrix, increasing the resistance of dislocation slip and climbing, impeding the migration of grain boundaries and improving the effect of recrystallization temperature and microstructure thermal stability [21,22,33,55,61,62]. In addition, Sc has the effect of refining α-Al grains [30–33,57,63–65].

Sc exists in aluminum alloys in two forms, solute atoms and $Al_3Sc$ particles [21,57,59], and the mechanism of refinement is also different. With regard to solute atoms, during the crystallization process, supersaturated Sc atoms are drained from the grains and biased at the front end of the solid–liquid interface, resulting in supercooling of the components, providing a degree of supercooling and inhibiting the growth of grains [57,59]. This refinement effect is due to the fact that the growth limiting factor of Sc is $3.9C_0$. As the core of heterogeneous nucleation [21,32], the $Al_3Sc$ phase significantly improves the nucleation rate, promotes α-Al grain nucleation and leads to grain refinement. This is because the $Al_3Sc$ phase has an $L1_2$ structure with a lattice constant of 0.4104 nm [55], which is very similar to Al in terms of face-centered cubic structure and lattice constant (0.4049 nm), and there is a small lattice mismatch(1.32% [55]) between the two phases.

The grain refining mechanism of Sc is different, which leads to the difference in the refining effect of α-Al grains. According to the results of literature studies [57,65], the refining effect of $Al_3Sc$ is stronger than that of solute atoms. As can be seen from Figure 2a, the grain size of α-Al without addition of Sc element is 860 μm. When 0.2 wt.%Sc is added, the grain size of α-Al is 830 μm, the grain size is coarse and uneven (Figure 3a) and there is no significant reduction in grain size. The grain refining effect is gradually enhanced with the increase in Sc content within eutectic composition (Sc = 0.58 wt.% Figure 2b). The grain size of 0.5 wt.%Sc alloy is 700 μm, and the grain size reduction is 160 μm. The grain size reduction rate is 18.6%. When Sc content is increased beyond the eutectic point, grain size decreases more significantly. An addition of 0.7 wt.% Sc can refine the grain to 40 μm. Figure 3b shows that the grain size is fine and uniform, and the reduction rate reaches 95.3%. This difference in refinement results from refinement mechanism. According to the Al-Sc binary phase diagram (Figure 2b), when the addition amount of Sc is lower than that of eutectic component, Sc element exists in the matrix in the form of solute atoms, and component subcooling is used as the mechanism of grain refinement. Beyond the eutectic point, $Al_3Sc$ begins to be the main form of Sc. At the same time, the refinement mechanism changes from the subcooling of solute atoms to heterogeneous nucleation. Heterogeneous nucleation has a stronger refinement effect and can significantly refine α-Al grains.

However, the refinement theory and optimization of refinement effect of $Al_3Sc$ need further study. The current understanding of grain refinement mechanism still remains the lattice mismatch proposed in 1952. In 2005, Zhang [66–68] proposed the E2E model to deeply understand the crystallographic relationship between heterogeneous phases and matrix. In 2021, Yan [65] found that there was a good orientation relationship between $Al_3Sc$ and α-Al:

$$[011]_{Al}//[011]_{Al_3Sc}\&(\bar{2}00)_{Al}//(\bar{2}00)_{Al_3Sc} \text{ and } [\bar{1}12]_{Al}//[\bar{1}12]_{Al_3Sc}\&(\bar{1}1\bar{1})_{Al}//(\bar{1}1\bar{1})_{Al_3Sc}$$

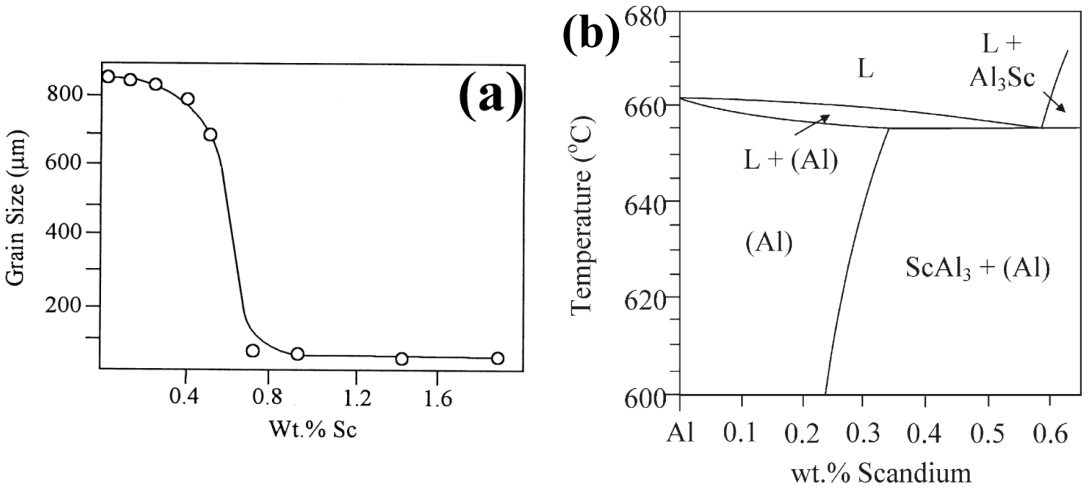



**Figure 2.** Curve of grain size addition of Sc [57] (**a**) and phase diagram of Al-Sc [57] (**b**). Reprinted with permission from [57], 1998, Elsevier.

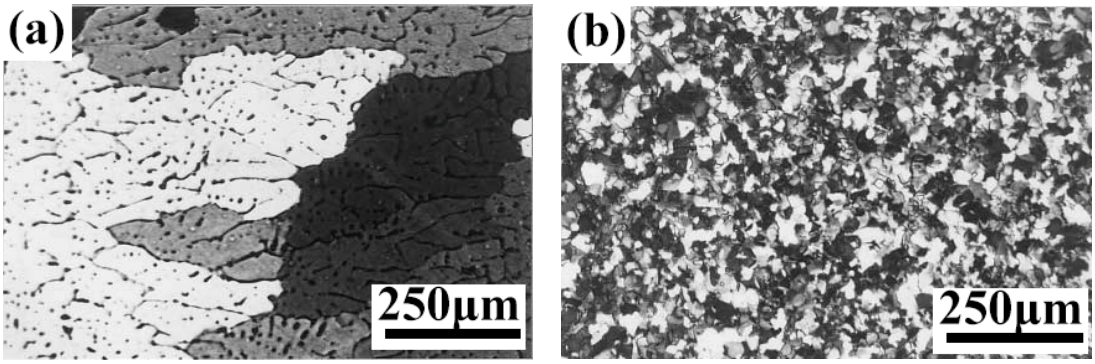



**Figure 3.** Optical microstructure (OM) structure [57]: (**a**) Al-0.2Sc, (**b**) Al-0.7Sc. Reprinted with permission from [57], 1998, Elsevier.

However, the crystallographic study of $Al_3Sc$ grain refinement has not been studied enough. In addition, the grain refinement effect is affected by the morphology, and the primary phase $Al_3Sc$ has many morphologies [69,70]. Sun [69] studied the relationship between melting conditions and the morphology of primary phase $Al_3Sc$, and found that cooling rate was the key factor affecting the morphology evolution of $Al_3Sc$. Melting temperature had a greater effect on the dendrite degree, and holding time had a greater effect on the primary phase size. Moderate melting temperature and rapid cooling result in the diversity of primary $Al_3Sc$ phase morphology, and this $Al_3Sc$ has the best refining effect on the studied alloys. Higher melting temperature and slower cooling rate will result in the primary $Al_3Sc$ phase with butterfly shape and cracked cube with pointed arrows at the corners, and the refining effect of this master alloy will be significantly reduced. Very low cooling rate and high melting temperature lead to dendrite formation of primary $Al_3Sc$ phase with the worst thinning effect and microstructure inheritance.

### *3.2. Al-Zr*

Zr, as a transition group element, is added to magnesium alloy in the form of Mg-Zr master alloy, which can produce strong grain refinement effect [71,72]. Zr has also been reported to refine α-Al grains [28–30,63,64].

Zr exists in different forms in aluminum alloys [28], and its refining mechanism is also different. According to the Al-Zr phase diagram [73], the solid solubility of Zr is 0.11 wt.%, and Zr exists in the form of solute atoms at this concentration. According to Table 1, the GRF of Zr is $6.8C_0$, and the segregation at the solid–liquid interface during

crystallization leads to the undercooling of the components. This reduces the undercooling degree, inhibiting the grain growth and refining the grains. In the presence of the $Al_3Zr$ phase, the mechanism of grain refinement is heterogeneous nucleation, which can be explained by Zhang Mingxing's Edge To Edge model [41,67,68]. The $Al_3Zr$ phase formed during the solidification process is a $D0_{23}$ crystal structure, belonging to the tetragonal crystal structure, with lattice constants of a = 0.4007 nm and c = 1.7286 nm. Each cell contains 12 Al atoms and 4 Zr atoms [74].

The most densely packed facet of the $Al_3Zr$ phase is $\{114\}_{Al_3Zr}$ that contains three densely packed atomic columns($< 22\bar{1} >^{S}_{Al_3Zr}$, $< 110 >^{Z}_{Al_3Zr}$ and $< 40\bar{1} >^{Z}_{Al_3Zr}$). For convenience, the superscript "Straight (for short, S)" and "Zig-Zag(for short, Z)" are used to distinguish the straight row atomic arrangement from the sawtooth row atomic arrangement, as shown in Figure 4a,b. A sub-densely packed plane is $\{020\}_{Al_3Zr}$, which contains only one dense row of atoms ($< 40\bar{1} >^{Z}_{Al_3Zr}$). The third densely packed surface of the $Al_3Zr$ phase is $\{220\}_{Al_3Zr}$, which contains two densely packed atomic columns ($< 22\bar{1} >^{S}_{Al_3Zr}$ and $< 110 >^{Z}_{Al_3Zr}$).

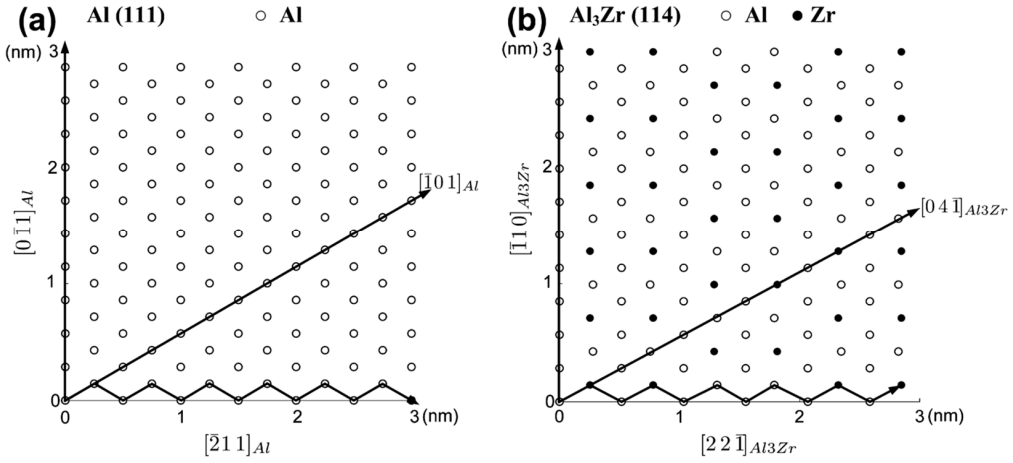



**Figure 4.** Schematic diagram of the arrangement of atoms [28]: (**a**) Al, (**b**) $Al_3Zr$. Reprinted with permission from [28], 2013, Elsevier.

Aluminum is a face-centered cubic structure with a lattice constant of a = 0.4049 nm and 4 Al atoms in the cell [74]. The most densely packed surface of Al is $\{111\}_{Al}$. It has two closely packed columns of atoms: $< 110 >^{Z}_{Al}$ and $< \bar{2}11 >^{S}_{Al}$. Furthermore, $\{020\}_{Al}$ is a sub-dense plane with only one dense row of atoms ($< 110 >^{Z}_{Al}$). The third closest plane is $\{220\}_{Al}$ containing $< 110 >^{Z}_{Al}$ and $< \bar{2}11 >^{S}_{Al}$.

The interatomic spacing mismatch and interplanar spacing mismatch between $Al_3Zr$ and $\alpha$-Al were calculated respectively, and the results are shown in Table 2. Table 3 lists the orientation relationships that meet the conditions of interatomic spacing mismatch less than 10% and interplanar spacing mismatch less than 6%. EBSD results prove the existence of two groups of orientation relationships (Figure 5):

$$[101]_{Al}(11\bar{1})_{Al}//[1\bar{1}0]_{Al_3Zr}(114)_{Al_3Zr} \text{ and } [1\bar{1}0]_{Al}(11\bar{1})_{Al}//[40\bar{1}]_{Al_3Zr}(114)_{Al_3Zr}$$

**Table 2.** Result of calculations [28].

| Matching Crystal Direction | $f_r$ | Matching Crystal Plane | $f_d$ |
|---|---|---|---|
| $<110>^{S}_{Al} // <110>^{S}_{Al_3Zr}$ | 1% | $\{111\}_{Al}//\{114\}_{Al_3Zr}$ | 1% |
| | | $\{111\}_{Al}//\{020\}_{Al_3Zr}$ | 17% |
| | | $\{111\}_{Al}//\{220\}_{Al_3Zr}$ | 65% |
| $<110>^{S}_{Al} // <40\bar{1}>^{S}_{Al_3Zr}$ | 2% | $\{020\}_{Al}//\{114\}_{Al_3Zr}$ | 15% |
| | | $\{020\}_{Al}//\{020\}_{Al_3Zr}$ | 1% |
| | | $\{020\}_{Al}//\{220\}_{Al_3Zr}$ | 42% |
| $<\bar{2}11>^{Z}_{Al} // <22\bar{1}>^{Z}_{Al_3Zr}$ | 4% | $\{022\}_{Al}//\{114\}_{Al_3Zr}$ | 40% |
| | | $\{022\}_{Al}//\{020\}_{Al_3Zr}$ | 29% |
| | | $\{020\}_{Al}//\{220\}_{Al_3Zr}$ | 1% |

**Table 3.** Orientation relationship between $Al_3Zr$ phase and α-Al [28].

| Matching Crystal Direction | $f_r$ | Matching Crystal Plane | $f_d$ |
|---|---|---|---|
| $<110>^{S}_{Al} // <110>^{S}_{Al_3Zr}$ | 1% | $\{111\}_{Al}//\{114\}_{Al_3Zr}$ | 1% |
| | | $\{022\}_{Al}//\{220\}_{Al_3Zr}$ | 1% |
| $<110>^{S}_{Al} // <40\bar{1}>^{S}_{Al_3Zr}$ | 2% | $\{111\}_{Al}//\{114\}_{Al_3Zr}$ | 1% |
| | | $\{020\}_{Al}//\{020\}_{Al_3Zr}$ | 1% |
| $<\bar{2}11>^{Z}_{Al} // <22\bar{1}>^{Z}_{Al_3Zr}$ | 4% | $\{111\}_{Al}//\{114\}_{Al_3Zr}$ | 1% |
| | | $\{022\}_{Al}//\{220\}_{Al_3Zr}$ | 1% |

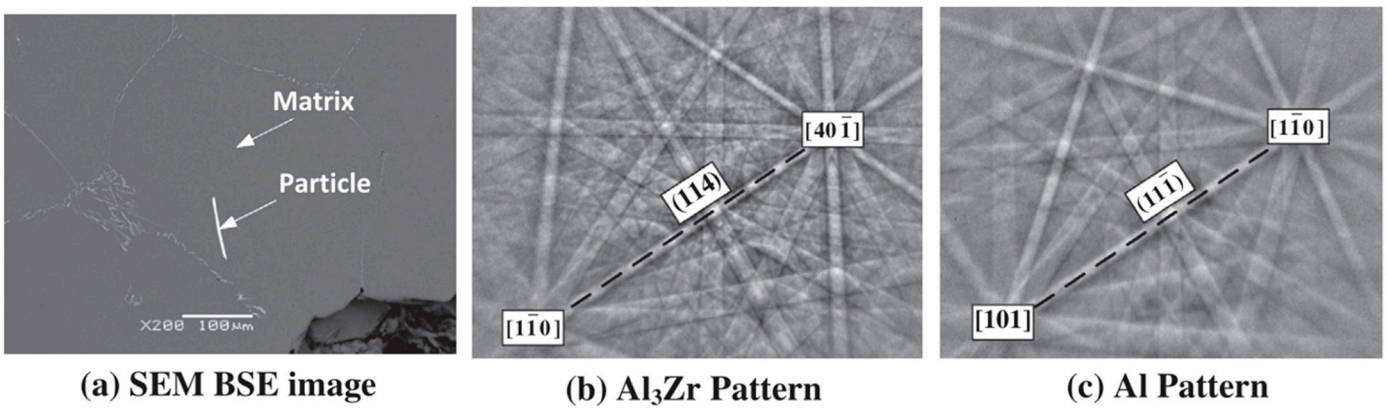



**Figure 5.** Backscattered electronic (BSE) image of the microstructure and EBSD Kikuchi pattern of $Al_3Zr$ and Al [28]. Reprinted with permission from [28], 2013, Elsevier.

The grain refinement mechanisms of solute atom Zr and $Al_3Zr$ are different, which leads to the difference in grain refinement effect. The refining effect of $Al_3Zr$ phase is much better than that of solute atomic Zr, which occupies a dominant position. Wang et al. [28] studied the effect of Zr addition on grain refinement of pure aluminum. The results show that the equilibrium solidification microstructure is obtained by controlling the cooling rate at 1 K/s when the addition amount is 0.1 wt.% (Figure 6b,e). It was found that the pure Al grain size is reduced from 1100 μm to 1050 μm (Figure 6a,e), and the grain size reduction rate is 4.5%. The grain size of pure aluminum is 500 μm and the size reduction rate is 54.5% when the addition amount is increased to 0.2 wt.% (Figure 6c,e). The addition was further increased to 0.5 wt.%, and the grain size was reduced to 350 μm (Figure 6e). This difference in refinement results from the change of refinement mechanism. When 0.1 wt.%Zr is added, the constitutional undercooling of solute atomic Zr acts as a refinement mechanism. If the addition amount of Zr is above 0.1 wt.%, $Al_3Zr$ is detected by XRD and serves as the core of α-Al nucleation.

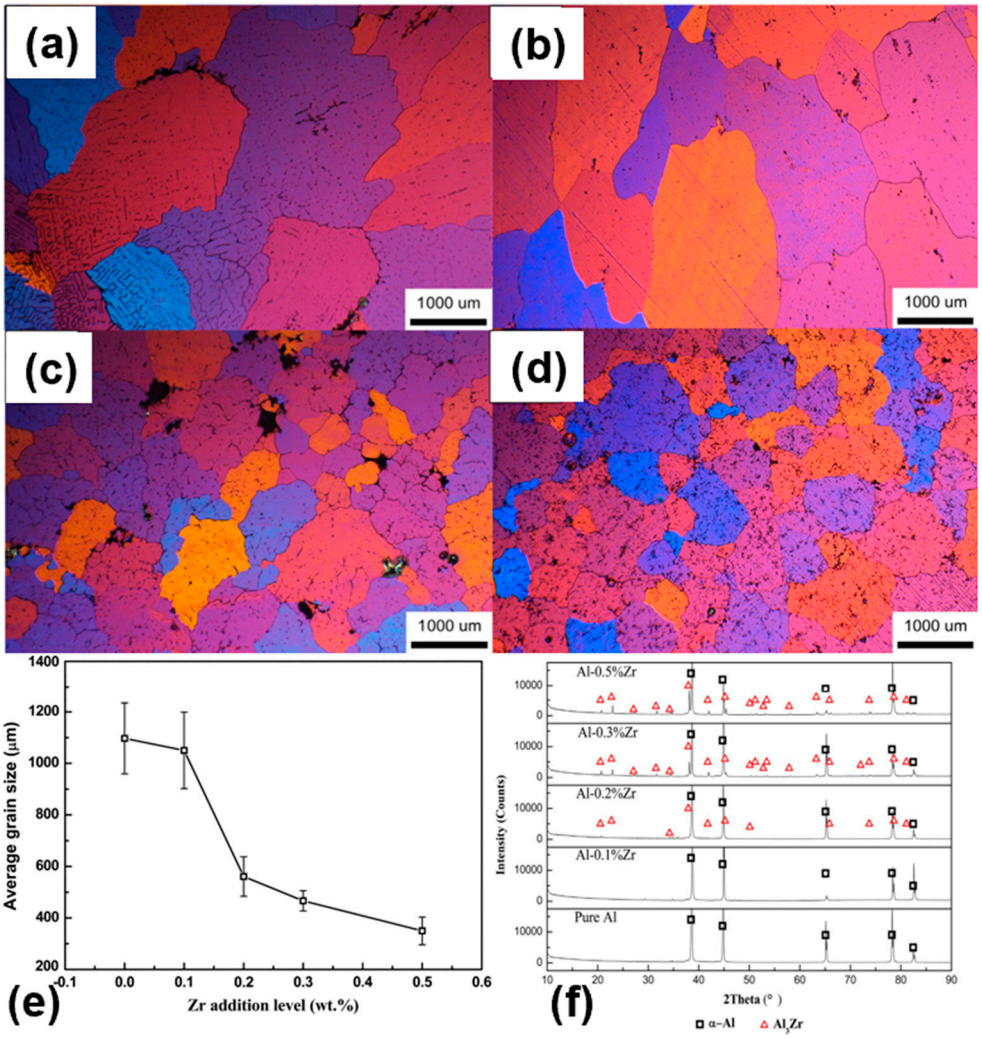



**Figure 6.** Results of grain refinement [28]: (**a**) 0% Zr, (**b**) 0.1% Zr, (**c**) 0.2% Zr, (**d**) 0.3% Zr, (**e**) relationship of Al grain size and Zr addition level, (**f**) XRD result of as-cast Al. Reprinted with permission from [28], 2013, Elsevier.

The refining effect of heterogeneous phase is affected by its morphology [75,76]. Through literature research, it was found that the morphology of $Al_3Zr$ will change according to different casting temperature [76]. When the temperatures were 1123 K, 1173 K, 1223 K and 1273 K, the morphologies of the $Al_3Zr$ of spherical shape, tetragon shape, rod shape and fiber shape were observed, respectively. At present, the effect of different $Al_3Zr$ morphologies on the refinement results has not been reported. The study on the effect of morphology on refinement has a positive effect on the optimization of refinement ability.

### *3.3. Al-Er*

The price of Er is only $\frac{1}{80}$~$\frac{1}{100}$ that of Sc [77], and the Er element is often added to aluminum alloy as an alternative element of Sc to produce microalloying and improve the microstructure and mechanical properties of the alloy [26,27,78–80]. As a rare earth element, a refined grain is one of the characteristics of Er [27,60,81].

Er exists in aluminum alloy in two forms: solute atom and $Al_3Er$ phase. Based on the literature review [27,60,81], the solute atom Er can only refine the α-Al dendrite arms, while the primary $Al_3Er$ phase can refine the grains. Wen et al. [27] studied the effect of refining as-cast Al-Mg-Mn-Zr alloys with different additions of Er, and observed that the addition of 0.2 wt.%Er did not lead to grain refinement compared with the alloys without Er. However, as shown in Figure 7b, there does appear to be refinement in the dendritic substructure

within the grains. The grain size of $\alpha$-Al decreased significantly after adding 0.4 wt.%Er. By comparison with Figure 7a,c, the grain size of the alloy containing 0.4 wt.%Er is only half of that without the addition of the alloy. Increasing the addition of Er will only lead to slight decrease in grain size. Figure 8 shows the XRD diffraction patterns of the as-cast alloy with different Er content and the homogenized alloy with 0.4 wt.%Er added. The peak of $Al_3Er$ phase appeared only after 0.4 wt.%Er was added, and the diffraction peak still existed after homogenization. However, this indicates that 0.2 wt.% Er can be dissolved in the matrix. In summary, according to the Al-Er phase diagram [82], the maximum solid solubility of Er is 0.05 wt.%, and XRD results show that there is no formation of $Al_3Er$ in the alloy added 0.2 wt.%Er. In the solidification process, the supersaturated Er is segregated at the grain boundary, but the GRF of Er is $0.88C_0$, which is much smaller than that of Zr ($6.8C_0$) and Sc ($3.9C_0$), so it is difficult to produce a refinement effect. At 0.4 wt.%, the presence form of Er changes, with solute atoms and intermetallic compounds co-existing. Except for a small part of Er that is dissolved in the matrix, most Er is segregated at the front end of the solid–liquid interface. The aggregation of Er at the interface will make the composition fluctuation near the interface more drastic, because in the Al-Er binary phase diagram, the eutectic reaction temperature at the Al-rich end is 655 °C, and the eutectic composition is 6 wt.%. When the melt near the solid–liquid interface is cooled to 655 °C, $Al_3Er$ compounds can be formed in the melt with high erbium content (more than eutectic point composition) near the interface. These $Al_3Er$ compounds are directly extracted from the melt. When the primary $Al_3Er$ phase appears in the melt, there is still much liquid that has failed to crystallize and nucleate. The lattice type ($L1_2$) and lattice constant (a = 0.4215 nm) of $Al_3Er$ are very close to that of aluminum matrix (face-centered cubic structure, lattice constant a = 0.4049 nm), and the lattice mismatch is 4.10% [81]. The two phases are congruent and semi-congruent. Moreover, the melting point of $Al_3Er$ is 1067 °C, which is much higher than the melting point of the matrix (660 °C), and it has good stability after formation and will not melt back into the matrix. These characteristics ensure that the $Al_3Er$ phase has a good heterogeneous nucleation, so the primary $Al_3Er$ phase can serve as the nucleation core and play a role in refining grains when the melt continues to crystallize and nucleate.

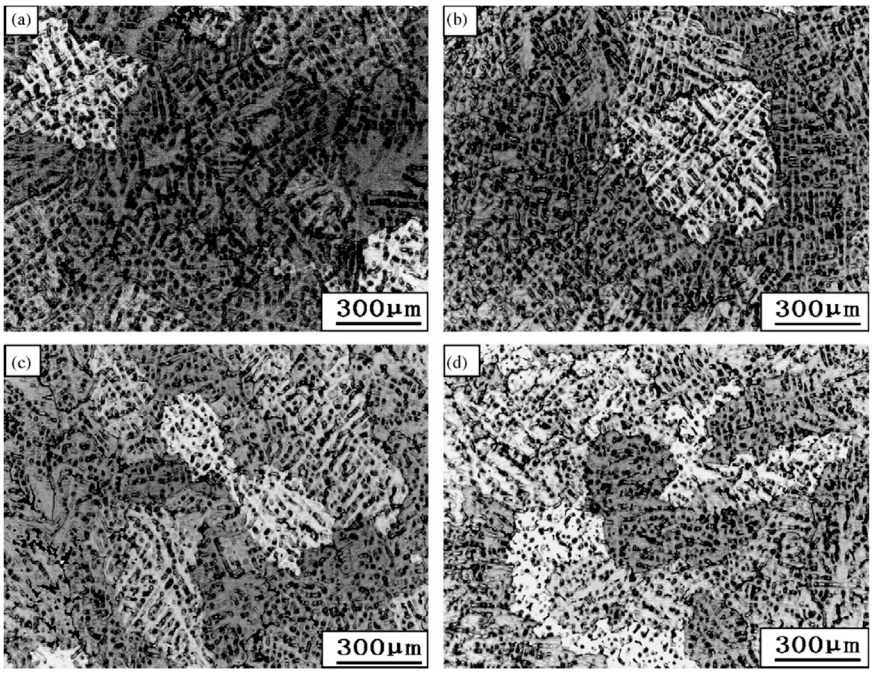



**Figure 7.** OM microstructure of as-cast Al-Mg-Mn-Zr-Er alloy [27]: (**a**) 0Er, (**b**) 0.2 wt.%Er, (**c**) 0.4 wt.%Er, (**d**) 0.6 wt.%Er. Reprinted with permission from [27], 2009, Elsevier.

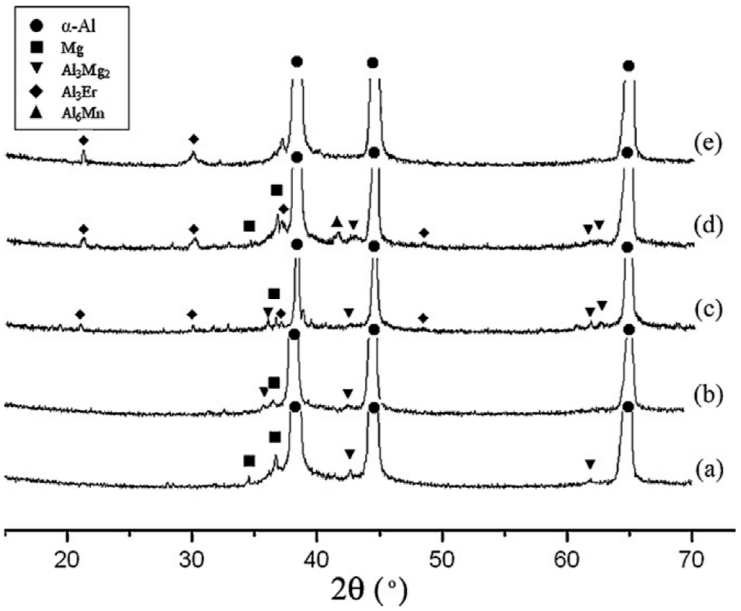



**Figure 8.** XRD diffraction patterns of as-cast alloys [27]: (**a**) 0Er, (**b**) 0.2 wt.%Er, (**c**) 0.4 wt.%Er, (**d**) 0.6 wt.%Er, (**e**) homogenized with 0.4 wt.%Er. Reprinted with permission from [27], 2009, Elsevier.

The primary phase has excellent thermal stability. Wen et al. [27] found that 0.2 wt.%Er was dissolved in the Al matrix as a solid solution, while other excess Er atoms were segregated at grain boundaries during solidification to form the main $Al_3Er$ phase. After homogenizing the cast alloy at 470 °C for 24 h (Figure 8), the morphology and structure of the primary $Al_3Er$ did not change, indicating that $Al_3Er$ could not dissolve into the Al matrix at this temperature because the melting point of $Al_3Er$ is much higher than the melting point of Al alloy. Although $Al_3Er$ can refine grains and has good thermal stability, Sc is an excellent candidate for intermediate alloys considering the crystal constant, lattice mismatch and growth limiting factor of $Al_3Sc$.

### *3.4. Al-Sc-Zr*

Based on the previous analysis of refinement mechanism and refinement effect of elements, Sc, Er and Zr all have the effect of refining grains. By forming primary $Al_3M$ phase and using heterogeneous nucleation as grain refining mechanism, they can all be used as candidate elements for preparing Al-M intermediate alloys.

The compound addition of elements in pairs is a means to improve the refining effect and reduce the amount and cost of rare earth addition. Studies have shown that the addition of Sc and Zr can significantly refine α-Al grains in aluminum alloys [33,63]. Yin et al. [63] studied the effect of compound addition of Sc and Zr on the casting microstructure of Al-Mg alloy. The results show that, compared with adding Sc and Zr separately, adding 0.2 wt.%Sc and 0.1 wt.%Zr to Al-5Mg alloy at the same time, the grain size of the alloy decreases more obviously, and the equiaxed grains are more uniform. Zou et al. [83] also found through experiments that the compound addition of trace Sc and Zr can better refine the grain of cast aluminum alloy. In addition, the combination of Sc and Zr elements can reduce the use of Sc elements, thus reducing the production cost. Meng et al. [64] studied the effect of rare earth Sc and Zr on the microstructure of Al-Mg-Si-Cu-Cr-V alloy, and found that the improvement effect of 0.13 wt.%Zr and 0.03 wt.%Sc added at the same time is almost the same as that of 0.15 wt.%Sc. Esmaeili et al. [84] found similar grain refinement in Al-Mg-Si-Sc-Zr alloys and reached the same conclusion. It is generally believed that the compound addition of Sc and Zr can produce a synergistic effect, that is, the precipitation strengthening effect of the $Al_3(Sc, Zr)$ phase formed by the decomposition of supersaturated solid solution is introduced to strengthen the matrix better [85–87]. Recent studies [88] indicate that controlling the mass ratio of Sc and Zr can change the primary phase type.

Wang [88] found $Al_3$(Sc, Zr) in the cast aluminum alloy after refining, where the mass ratio of Sc and Zr is 1, and the addition amount is 0.2 wt.%. When the mass ratio of Sc to Zr was adjusted to 4 and the addition amount of Zr was 0.1 wt.%, the cast microstructure was only $Al_3Sc$, and their composite phase was not detected [89]. The mass ratio of Sc to Zr was adjusted to 0.5, the addition amount of Zr was 0.2 wt.%, the cast microstructure was only $Al_3Sc$, and their composite phase was not detected [90]. Compared to $Al_3Sc$, $Al_3$(Sc, Zr) is also an $L1_2$ structure with a smaller lattice mismatch (1.15%) with Al [91].Further analysis shows that by regulating the mass ratio of Sc and Zr, the primary phase type changes and the mechanism of grain refinement is different, which appears in Al-V-B [92].Whether the size, morphology and distribution will change needs to be further studied.

## 4. Prospects

Aluminum alloy with light weight, excellent mechanical properties, corrosion resistance and conductive properties are used in aerospace, ships, transportation and other fields. Due to the influence of casting process parameters and environmental factors, the organization and composition of cast aluminum parts are not uniform, which limits the expansion of the application range of aluminum alloy. In order to solve this problem, based on the idea of screening out $Al_2RE$ in magnesium alloy, which can refine grain and improve thermal stability of microstructure, this paper proposes the idea of preparing a new Al-M master alloys with grain refinement and a microalloying effect, which can not only solve the uneven structure and composition of casting, but also produce a microalloying effect after refining. This further improves the heat resistance of aluminum alloy. The selection of elements suitable for the preparation of new master alloys, the discussion of the refinement mechanism of elements, the analysis of the refinement effect of elements and the summary of factors affecting the refinement effect have very important theoretical significance for understanding the nature of the chemical method affecting the refinement of the grain, and its application in industrial production and guidance of the development of intermediate alloys, but also has practical application value. We selected Sc and Zr elements as reference objects for Al-M master alloys, but there are still many problems:

(1) The refinement mechanism of $Al_3Sc$ needs further analysis. At present, the understanding of the refinement mechanism is still in the crystal structure, lattice constant and lattice mismatch. With the help of E2E model, it is helpful to explore the crystallographic relationship between $Al_3Sc$ and α-Al and to improve the refinement theory. Sc is a eutectic reaction type element, and the primary $Al_3Sc$ phase in the eutectic structure during the solidification process is isolated at the grain boundary. The influence of the size, distribution and number density of the primary phase on the refining effect is still unclear.

(2) The primary $Al_3Zr$ phase will have different morphologies when the melting conditions are different. The law and mechanism of the influence of morphologies on the refining effect need to be explored using experiments. The size and distribution of the primary phase are also factors to be considered.

(3) The analysis of the strength of the grain refinement effect of Sc and Zr elements can provide data in support of the optimization of the refinement effect and the design of ternary alloy composition.

(4) When the pairwise addition of Sc and Zr elements to prepare ternary master alloys is performed, the primary phase type of the master alloys is affected by the mass ratio of Sc and Zr, and whether the morphology and distribution will have the same law. Whether the composition ratio of Sc and Zr is also one of the factors affecting the type, morphology and distribution of primary phase is still to be discussed. In addition, if the type and morphology of primary phase change, will the refinement mechanism also change?

**Author Contributions:** Conceptualization, Z.L. and S.W.; methodology, Z.L.; formal analysis, Z.L.; investigation, Z.L.; resources, S.W., H.H., W.W. and Z.N.; data curation, Z.L.; writing—original draft

preparation, Z.L.; writing—review and editing, Z.L., S.W.; visualization, S.W.; supervision, S.W. and Z.N.; project administration, W.W.; funding acquisition, S.W., H.H. and Z.N. All authors have read and agreed to the published version of the manuscript.

**Funding:** National key Research and Development Program of China (Nos.2021YFB370902, 2021YFB3-704204 and 2021YFB3704205), National Natural Science Foundation of China for Innovation Research Project(No.51621003).

**Data Availability Statement:** Not applicable.

**Conflicts of Interest:** The authors declare no conflict of interest.

## References

1. McCartney, D.G. Grain refining of aluminium and its alloys using inoculants. *Int. Mater. Rev.* **1989**, *34*, 247–260. [CrossRef]
2. Ralston, K.D.; Birbilis, N. Effect of Grain Size on Corrosion: A Review. *Corrosion* **2010**, *66*, 319–324. [CrossRef]
3. Nowak, M.; Bolzoni, L.; Hari Babu, N. Grain refinement of Al–Si alloys by Nb–B inoculation. Part I: Concept development and effect on binary alloys. *Mater. Des.* **2015**, *66*, 366–375. [CrossRef]
4. Langdon, T.G. Twenty-five years of ultrafine-grained materials: Achieving exceptional properties through grain refinement. *Acta Mater.* **2013**, *61*, 7035–7059. [CrossRef]
5. Karbalaei Akbari, M.; Baharvandi, H.R.; Shirvanimoghaddam, K. Tensile and fracture behavior of nano/micro $TiB_2$ particle reinforced casting A356 aluminum alloy composites. *Mater. Des.* **2015**, *66*, 150–161. [CrossRef]
6. Wang, M.; Chen, D.; Chen, Z.; Wu, Y.; Wang, F.; Ma, N.; Wang, H. Mechanical properties of in-situ $TiB_2$/A356 composites. *Mater. Sci. Eng. A* **2014**, *590*, 246–254. [CrossRef]
7. Zhao, K.; Gao, T.; Yang, H.; Hu, K.; Liu, G.; Sun, Q.; Nie, J.; Liu, X. Enhanced grain refinement and mechanical properties of a high–strength Al–Zn–Mg–Cu–Zr alloy induced by TiC nano-particles. *Mater. Sci. Eng. A* **2021**, *806*, 140852. [CrossRef]
8. Ali, Y.; Qiu, D.; Jiang, B.; Pan, F.; Zhang, M.X. Current research progress in grain refinement of cast magnesium alloys: A review article. *J. Alloys Compd.* **2015**, *619*, 639–651. [CrossRef]
9. Wannasin, J.; Canyook, R.; Wisutmethangoon, S.; Flemings, M.C. Grain refinement behavior of an aluminum alloy by inoculation and dynamic nucleation. *Acta Mater.* **2013**, *61*, 3897–3903. [CrossRef]
10. Tamirisakandala, S.; Bhat, R.B.; Tiley, J.S.; Miracle, D.B. Grain refinement of cast titanium alloys via trace boron addition. *Scr. Mater.* **2005**, *53*, 1421–1426. [CrossRef]
11. Murty, B.S.; Kori, S.A.; Chakraborty, M. Grain refinement of aluminium and its alloys by heterogeneous nucleation and alloying. *Int. Mater. Rev.* **2002**, *47*, 3–29. [CrossRef]
12. Fan, Z.; Wang, Y.; Zhang, Y.; Qin, T.; Zhou, X.R.; Thompson, G.E.; Pennycook, T.; Hashimoto, T. Grain refining mechanism in the Al/Al–Ti–B system. *Acta Mater.* **2015**, *84*, 292–304. [CrossRef]
13. Wang, T.; Chen, Z.; Fu, H.; Xu, J.; Fu, Y.; Li, T. Grain refining potency of Al–B master alloy on pure aluminum. *Scr. Mater.* **2011**, *64*, 1121–1124. [CrossRef]
14. Zhang, M.X.; Kelly, P.M. Accurate orientation relationships between ferrite and cementite in pearlite. *Scr. Mater.* **1997**, *37*, 2009–2015. [CrossRef]
15. Zhang, M.X.; Kelly, P.M.; Easton, M.A.; Taylor, J.A. Crystallographic study of grain refinement in aluminum alloys using the edge-to-edge matching model. *Acta Mater.* **2005**, *53*, 1427–1438. [CrossRef]
16. Dai, J.; Zhu, S.; Easton, M.A.; Zhang, M.; Qiu, D.; Wu, G.; Liu, W.; Ding, W. Heat treatment, microstructure and mechanical properties of a Mg–Gd–Y alloy grain-refined by Al additions. *Mater. Sci. Eng. A* **2013**, *576*, 298–305. [CrossRef]
17. Qiu, D.; Zhang, M.X.; Taylor, J.A.; Kelly, P.M. A new approach to designing a grain refiner for Mg casting alloys and its use in Mg–Y-based alloys. *Acta Mater.* **2009**, *57*, 3052–3059. [CrossRef]
18. Luo, Y.; Zhou, L.; Kang, M.; Peng, G.; Li, W.; Miao, S.; Huang, Y.; Zhao, Y.; Xu, Y. Effect of Warm Rolling on the Grain-Refining Performance of Al-5Ti-1B Grain Refiner in Al. *JOM* **2022**, *74*, 1210–1217. [CrossRef]
19. Li, Z.; Hu, B.; Li, D.; Zhang, W.; Zeng, X.; Lin, Z.; Jin, C.; Zhao, S. Microstructure-dependent thermal conductivity and mechanical properties in cast Mg-4Sm-xAl alloys. *Mater. Sci. Eng. A* **2022**, *861*, 144336. [CrossRef]
20. Li, H.-Y.; Li, D.-W.; Zhu, Z.-X.; Chen, B.-A.; Chen, X.; Yang, C.-L.; Zhang, H.-Y.; Kang, W. Grain refinement mechanism of as-cast aluminum by hafnium. *Trans. Nonferrous Met. Soc. China* **2016**, *26*, 3059–3069. [CrossRef]
21. Chuvil'deev, V.N.; Shadrina, I.S.; Nokhrin, A.V.; Kopylov, V.I.; Bobrov, A.A.; Gryaznov, M.Y.; Shotin, S.V.; Tabachkova, N.Y.; Chegurov, M.K.; Melekhin, N.V. An investigation of thermal stability of structure and mechanical properties of Al-0.5Mg–Sc ultrafine-grained aluminum alloys. *J. Alloys Compd.* **2020**, *831*, 154805. [CrossRef]
22. Min, B.K.; Kim, H.W.; Kang, S.B. Effect of $Al_3Sc$ precipitate on the microstructural evolution during accumulative roll bonding in Al–0.2wt.% Sc alloy. *J. Mater. Process. Technol.* **2005**, *162*, 355–361. [CrossRef]
23. Knipling, K.E.; Dunand, D.C. Creep resistance of cast and aged Al–0.1Zr and Al–0.1Zr–0.1Ti (at.%) alloys at 300–400 °C. *Scr. Mater.* **2008**, *59*, 387–390. [CrossRef]
24. Knipling, K.E.; Dunand, D.C.; Seidman, D.N. Nucleation and Precipitation Strengthening in Dilute Al-Ti and Al-Zr Alloys. *Metall. Mater. Trans. A* **2007**, *38*, 2552–2563. [CrossRef]

25. Su, N.; Guan, R.; Wang, X.; Wang, Y.; Jiang, W.; Liu, H. Grain refinement in an AlEr alloy during accumulative continuous extrusion forming. *J. Alloys Compd.* **2016**, *680*, 283–290. [CrossRef]
26. Wen, S.P.; Gao, K.Y.; Li, Y.; Huang, H.; Nie, Z.R. Synergetic effect of Er and Zr on the precipitation hardening of Al–Er–Zr alloy. *Scr. Mater.* **2011**, *65*, 592–595. [CrossRef]
27. Wen, S.P.; Xing, Z.B.; Huang, H.; Huang, H.; Nie, Z.R. The effect of erbium on the microstructure and mechanical properties of Al–Mg–Mn–Zr alloy. *Mater. Sci. Eng. A* **2009**, *516*, 42–49. [CrossRef]
28. Wang, F.; Qiu, D.; Liu, Z.-L.; Taylor, J.A.; Easton, M.A.; Zhang, M.-X. The grain refinement mechanism of cast aluminium by zirconium. *Acta Mater.* **2013**, *61*, 5636–5645. [CrossRef]
29. Gao, Z.; Li, H.; Lai, Y.; Ou, Y.; Li, D. Effects of minor Zr and Er on microstructure and mechanical properties of pure aluminum. *Mater. Sci. Eng. A* **2013**, *580*, 92–98. [CrossRef]
30. Wang, W.; Pan, Q.; Lin, G.; Wang, X.; Sun, Y.; Wang, X.; Ye, J.; Sun, Y.; Yu, Y.; Jiang, F.; et al. Microstructure and properties of novel Al-Ce-Sc, Al-Ce-Y, Al-Ce-Zr and Al-Ce-Sc-Y alloy conductors processed by die casting, hot extrusion and cold drawing. *J. Mater. Sci. Technol.* **2020**, *58*, 155–170. [CrossRef]
31. Tian, S.; Li, J.; Zhang, J.; Wulabieke, Z.; Lv, D. Effect of Zr and Sc on microstructure and properties of 7136 aluminum alloy. *J. Mater. Res. Technol.* **2019**, *8*, 4130–4140. [CrossRef]
32. Jiang, Y.; Liu, F. Effects of Sc or/and Ge addition on microstructure and mechanical properties of as-cast 6016 Al alloy. *J. Alloys Compd.* **2019**, *809*, 151829. [CrossRef]
33. Ocenasek, V.; Slamova, M. Resistance to recrystallization due to Sc and Zr addition to Al–Mg alloys. *Mater. Charact.* **2001**, *47*, 157–162. [CrossRef]
34. Wang, F.; Liu, Z.L.; Qiu, D.; Taylor, J.A.; Easton, M.A.; Zhang, M.X. The Influence of the Effect of Solute on the Thermodynamic Driving Force on Grain Refinement of Al Alloys. *Metall. Mater. Trans. A Phys. Metall. Mater. Sci.* **2015**, *46*, 505–515. [CrossRef]
35. Chen, Z.w.; He, Z.; Jie, W.q. Growth restriction effects during solidification of aluminium alloys. *Trans. Nonferrous Met. Soc. China* **2009**, *19*, 410–413. [CrossRef]
36. Easton, M.A.; StJohn, D.H. A model of grain refinement incorporating alloy constitution and potency of heterogeneous nucleant particles. *Acta Mater.* **2001**, *49*, 1867–1878. [CrossRef]
37. Greer, A.L.; Bunn, A.M.; Tronche, A.; Evans, P.V.; Bristow, D.J. Modelling of inoculation of metallic melts: Application to grain refinement of aluminium by Al–Ti–B. *Acta Mater.* **2000**, *48*, 2823–2835. [CrossRef]
38. Minouei, H.; Rizi, M.S.; Akbari, G.; Hong, S.I. Effect of residual nanocrystals on thermal stability and mechanical properties of metalloid-containing amorphous alloys. *Mater. Charact.* **2021**, *173*, 110914. [CrossRef]
39. Bruce, L.B. The effect of carbide and nitride additions on the eterogeneous nucleation behavior of liquid iron. *Metall. Trans.* **1970**, *1*, 1987–1995.
40. Turnbull, D.; Vonnegut, B. Nucleation Catalysis. *Ind. Eng. Chem.* **1952**, *44*, 1292–1298. [CrossRef]
41. Zhang, M.X.; Kelly, P.M.; Ma, Q.; Taylor, J.A. Crystallography of grain refinement in Mg–Al based alloys. *Acta Mater.* **2005**, *53*, 3261–3270. [CrossRef]
42. Xiao, F.; Wu, M.; Wang, Y.; Wang, S.; Shu, D.; Wang, D.; Zhu, G.; Mi, J.; Sun, B. Design of newly effective grain refiner for aluminum based on medium-entropy metal diboride. *Vacuum* **2022**, *205*, 111462. [CrossRef]
43. Li, G.-J.; Liao, H.-C. E2EM's prediction of $LaB_6$ as nucleation substrate for primary Mn-rich phase in Al-Si-Cu-Mn heat-resistant alloy and its refining effect. *Trans. Nonferrous Met. Soc. China* **2022**, *32*, 1795–1804. [CrossRef]
44. Sunitha, K.; Gurusami, K. Study of Al-Si alloys grain refinement by inoculation. *Mater. Today Proc.* **2021**, *43*, 1825–1829. [CrossRef]
45. Greer, A.L.; Cooper, P.S.; Meredith, M.W.; Schneider, W.; Schumacher, P.; Spittle, J.A.; Tronche, A. Grain refinement of aluminium alloys by inoculation. *Adv. Eng. Mater.* **2003**, *5*, 81–91. [CrossRef]
46. Johnsson, M. Grain refinement of aluminium studied by use of a thermal analytical technique. *Thermochim. Acta* **1995**, *256*, 107–121. [CrossRef]
47. Easton, M.; StJohn, D. An analysis of the relationship between grain size, solute content, and the potency and number density of nucleant particles. *Metall. Mater. Trans. A* **2005**, *36*, 1911–1920. [CrossRef]
48. Jing, L.-J.; Pan, Y.; Lu, T.; Pi, J.-H.; Gu, T.-F. Nucleation potency prediction of LaB6 with E2EM model and its influence on microstructure and tensile properties of Al-7Si-0.3Mg alloy. *Trans. Nonferrous Met. Soc. China* **2018**, *28*, 1687–1694. [CrossRef]
49. Guan, R.G.; Misra, R.D.K.; Shang, Y.; An, Y.; Wang, Y.; Zhang, Y.; Tie, D. Mechanism of microstructural refinement of deformed aluminum under synergistic effect of $TiAl_3$ and $TiB_2$ particles and impact on mechanical properties. *Mater. Sci. Eng. A* **2018**, *716*, 129–139. [CrossRef]
50. Han, Y.; Shu, D.; Wang, J.; Sun, B. Microstructure and grain refining performance of Al-5Ti-1B master alloy prepared under high-intensity ultrasound. *Mater. Sci. Eng. A* **2006**, *430*, 326–331. [CrossRef]
51. Xu, J.; Li, R.X.; Qian, L. Effect of Agglomeration on Nucleation Potency of Inoculant Particles in the Al-Nb-B Master Alloy: Modeling and Experiments. *Metall. Mater. Trans. A* **2021**, *52*, 1077–1094. [CrossRef]
52. Quested, T.E.; Greer, A.L. The effect of the size distribution of inoculant particles on as-cast grain size in aluminium alloys. *Acta Mater.* **2004**, *52*, 3859–3868. [CrossRef]
53. Greer, A.L. Grain refinement of alloys by inoculation of melts. *Philos. Trans. R. Soc. Lond. A* **2003**, *361*, 479–495. [CrossRef]
54. Yu, H.; Wang, N.; Guan, R.; Tie, D.; Li, Z.; An, Y.; Zhang, Y. Evolution of secondary phase particles during deformation of Al-5Ti-1B master alloy and their effect on α-Al grain refinement. *J. Mater. Sci. Technol.* **2018**, *34*, 2297–2306. [CrossRef]

55. Knipling, K.E.; Dunand, D.C.; Seidman, D.N. Criteria for developing castable, creep-resistant aluminum-based alloys—A review. *Int. J. Mater. Res.* **2006**, *97*, 246–265. [CrossRef]
56. Marcantonio, J.; Mondolfo, L. Nucleation of aluminium by several intermetallic compounds. *J. Inst. Met.* **1970**, *98*, 23–27.
57. Norman, A.F.; Prangnell, P.B.; McEwen, R.S. The solidification behaviour of dilute aluminium–scandium alloys. *Acta Mater.* **1998**, *46*, 5715–5732. [CrossRef]
58. Hu, X.W.; Jiang, F.G.; Ai, F.R. Effects of rare earth Er additions on microstructure development and mechanical properties of die-cast ADC12 aluminum alloy. *J. Alloys Compd.* **2012**, *538*, 21–27. [CrossRef]
59. Muhammad, A.; Cong, X.; Wang, X.J. High strength aluminum cast alloy: A Sc modification of a standard Al–Si–Mg cast alloy. *Mater. Sci. Eng. A* **2014**, *16*, 122–126. [CrossRef]
60. Yang, J.J.; Nie, Z.R.; Jin, T.N.; Ruan, H.Q.; Zuo, T.Y. Form and refinement mechanism of element Er in Al-Zn-Mg alloy. *Chin. J. Nonferrous Met.* **2004**, *4*, 620–626. (In Chinese) [CrossRef]
61. Jones, M.J.; Humphreys, F.J. Interaction of recrystallization and precipitation: The effect of $Al_3Sc$ on the recrystallization behaviour of deformed aluminium. *Acta Mater.* **2003**, *51*, 2149–2159. [CrossRef]
62. Riddle, Y.W.; Sanders, T.H. A study of coarsening, recrystallization, and morphology of microstructure in Al-Sc-(Zr)-(Mg) alloys. *Metall. Mater. Trans. A* **2004**, *35*, 341–350. [CrossRef]
63. Yin, Z.; Pan, Q.; Zhang, Y.; Jiang, F. Effect of minor Sc and Zr on the microstructure and mechanical properties of Al–Mg based alloys. *Mater. Sci. Eng. A* **2000**, *280*, 151–155. [CrossRef]
64. Meng, Y.; ZHAO, Z.H.; Cui, J.Z. Effect of minor Zr and Sc on microstructures and mechanical properties of Al–Mg–Si–Cu–Cr–V alloys. *Trans. Nonferrous Met. Soc. China* **2013**, *23*, 1882–1889. [CrossRef]
65. Yan, K.; Chen, Z.W.; Zhao, Y.N.; Ren, C.C.; Lu, W.J.; Aldeen, A.W. Morphological characteristics of Al3Sc particles and crystallographic orientation relationships of Al3Sc/Al interface in cast Al-Sc alloy. *J. Alloys Compd.* **2021**, *861*, 158491. [CrossRef]
66. Kelly, P.; Zhang, M.-X. Edge-to-edge matching—The fundamentals. *Metall. Mater. Trans. A* **2006**, *37*, 833–839. [CrossRef]
67. Zhang, M.X.; Kelly, P.M. Edge-to-edge matching and its applications: Part II. Application to Mg–Al, Mg–Y and Mg–Mn alloys. *Acta Mater.* **2005**, *53*, 1085–1096. [CrossRef]
68. Zhang, M.X.; Kelly, P.M. Edge-to-edge matching and its applications: Part I. Application to the simple HCP/BCC system. *Acta Mater.* **2005**, *53*, 1073–1084. [CrossRef]
69. Sun, Y.; Pan, Q.; Luo, Y.; Liu, Y.; Sun, Y.; Long, L.; Li, M.; Wang, X.; Liu, S. Study on the primary $Al_3Sc$ phase and the structure heredity of Al-Zn-Mg-Cu-Sc-Zr alloy. *Mater. Charact.* **2020**, *169*, 110601. [CrossRef]
70. Hyde, K.B.; Norman, A.F.; Prangnell, P.B. The effect of cooling rate on the morphology of primary $Al_3Sc$ intermetallic particles in Al–Sc alloys. *Acta Mater.* **2001**, *49*, 1327–1337. [CrossRef]
71. Qian, M.; Stjohn, D.H. Grain nucleation and formation in Mg–Zr alloys. *Int. J. Cast Met. Res.* **2009**, *22*, 256–259. [CrossRef]
72. Qian, M.; Das, A. Grain refinement of magnesium alloys by zirconium: Formation of equiaxed grains. *Scr. Mater.* **2006**, *54*, 881–886. [CrossRef]
73. Okamoto, H. Al-Zr (aluminum-zirconium). *J. Phase Equilibria* **2002**, *23*, 455–456. [CrossRef]
74. Villars, P.; Calvert, L.D. *Pearson's Handbook of Crystallographic Data for Intermetallic Phases*; ASM: Materials Park, OH, USA, 1991.
75. Han, Y.; Ke, L.; Wang, J.; Da, S.; Sun, B. Influence of high-intensity ultrasound on grain refining performance of Al–5Ti–1B master alloy on aluminium. *Mater. Sci. Eng. A* **2005**, *405*, 306–312. [CrossRef]
76. Zhao, Y.; Zhang, S.; Chen, G.; Cheng, X. Effects of molten temperature on the morphologies of in situ $Al_3Zr$ and $ZrB_2$ particles and wear properties of $(Al_3Zr+ZrB_2)$/Al composites. *Mater. Sci. Eng. A* **2007**, *457*, 156–161. [CrossRef]
77. Nie, Z.R.; Wen, S.P.; Huang, H.; Li, B.L.; Zuo, T.Y. Research progress of Er-containing aluminum alloy. *Chin. J. Nonferrous Met.* **2011**, *21*, 2361–2370. (In Chinese) [CrossRef]
78. Nie, Z.R.; Jin, T.N.; Zou, J.X.; Fu, J.B.; Yang, J.J.; Zuo, T.Y. Development on research of advanced rare-earth aluminum alloy. *Trans. Nonferrous Met. Soc. China* **2003**, *13*, 509–514.
79. Bai, S.; Liu, Z.; Li, Y.; Hou, Y.; Chen, X. Microstructures and fatigue fracture behavior of an Al–Cu–Mg–Ag alloy with addition of rare earth Er. *Mater. Sci. Eng. A* **2010**, *527*, 1806–1814. [CrossRef]
80. Lu, S.; Yin, D.; Zhao, Y.C.; Liu, C.; Zhao, M.C.; Yu, Z.; Wang, H.; Atrens, A. Evolution of microstructure and texture for an Al-0.4 Er alloy during accumulative roll bonding. *J. Alloys Compd.* **2019**, *811*, 152005. [CrossRef]
81. Yang, J.J.; Nie, Z.R.; Jin, T.N.; Xu, G.F.; Fu, J.B.; Ruan, H.Q.; Zuo, T.Y. Effect of trace rare earth element Er on high pure Al. *Trans. Nonferrous Met. Soc. China* **2003**, *5*, 1035–1039.
82. Mondolfo, L.F. Al–Er Aluminum–Erbium system. In *Aluminum Alloys*; Butterworth-Heinemann: Oxford, UK, 1976; p. 280. [CrossRef]
83. Zou, L.; Pan, Q.-L.; He, Y.-B.; Wang, C.-Z.; Liang, W.-J. Effect of minor Sc and Zr addition on microstructures and mechanical properties of Al-Zn-Mg-Cu alloys. *Trans. Nonferrous Met. Soc. China* **2007**, *17*, 340–345. [CrossRef]
84. Esmaeili Ghayoumabadi, M.; Mochugovskiy, A.G.; Tabachkova, N.Y.; Mikhaylovskaya, A.V. The influence of minor additions of Y, Sc, and Zr on the microstructural evolution, superplastic behavior, and mechanical properties of AA6013 alloy. *J. Alloys Compd.* **2022**, *900*, 163477. [CrossRef]
85. Knipling, K.E.; Seidman, D.N.; Dunand, D.C. Ambient- and high-temperature mechanical properties of isochronally aged Al–0.06Sc, Al–0.06Zr and Al–0.06Sc–0.06Zr (at.%) alloys. *Acta Mater.* **2011**, *59*, 943–954. [CrossRef]

86. Lee, S.; Utsunomiya, A.; Akamatsu, H.; Neishi, K.; Furukawa, M.; Horita, Z.; Langdon, T.G. Influence of scandium and zirconium on grain stability and superplastic ductilities in ultrafine-grained Al–Mg alloys. *Acta Mater.* **2002**, *50*, 553–564. [CrossRef]
87. Yuzbekova, D.; Mogucheva, A.; Kaibyshev, R. Superplasticity of ultrafine-grained Al–Mg–Sc–Zr alloy. *Mater. Sci. Eng. A* **2016**, *675*, 228–242. [CrossRef]
88. Wang, Y.; Zhang, Z.; Wu, R.; Sun, J.; Jiao, Y.; Hou, L.; Zhang, J.; Li, X.; Zhang, M. Ambient-temperature mechanical properties of isochronally aged 1420-Sc-Zr aluminum alloy. *Mater. Sci. Eng. A* **2019**, *745*, 411–419. [CrossRef]
89. Kuang, Q.; Wang, R.; Peng, C.; Cai, Z. Comparison of microstructure and mechanical properties of Al-Mg-Li-Sc-Zr alloys processed by ingot metallurgy and rapid solidification. *J. Alloys Compd.* **2021**, *883*, 160937. [CrossRef]
90. Zhang, X.; Zhang, L.; Wu, G.; Sun, J.; Rong, M.; Hsieh, C.-C.; Yu, Y. Influence of Sc content on the microstructure and mechanical properties of cast Al-2Li-2Cu-0.5Mg-0.2Zr alloy. *Mater. Charact.* **2018**, *142*, 223–236. [CrossRef]
91. Fuller, C.B.; Seidman, D.N.; Dunand, D.C. Mechanical properties of Al(Sc,Zr) alloys at ambient and elevated temperatures. *Acta Mater.* **2003**, *51*, 4803–4814. [CrossRef]
92. Zhao, C.; Li, Y.; Xu, J.; Luo, Q.; Jiang, Y.; Xiao, Q.; Li, Q. Enhanced grain refinement of Al-Si alloys by novel Al-V-B refiners. *J. Mater. Sci. Technol.* **2021**, *94*, 104–112. [CrossRef]


**Disclaimer/Publisher's Note:** The statements, opinions and data contained in all publications are solely those of the individual author(s) and contributor(s) and not of MDPI and/or the editor(s). MDPI and/or the editor(s) disclaim responsibility for any injury to people or property resulting from any ideas, methods, instructions or products referred to in the content.